FEATURE ARTICLE

Coarse-Grained Chemical Reaction Model

Yaroslava G. Yingling and Barbara J. Garrison*

Department of Chemistry, 152 Davey Laboratory, The Pennsylvania State University, University Park, Pennsylvania 16802

Received: June 18, 2003; In Final Form: November 17, 2003

We have developed a methodology for including effects of chemical reactions in coarse-grained computer simulations such as those that use the united atom approximation. The new coarse-grained chemical reaction model (CGCRM) adopts the philosophy of kinetic Monte Carlo approaches and includes a probabilistic element to predicting when reactions occur, thus obviating the need for a chemically correct interaction potential. The CGCRM uses known chemical reactions along with their probabilities and exothermicities for a specific material in order to assess the effect of chemical reactions on a physical process of interest. The reaction event in the simulation is implemented by removing the reactant molecules from the simulation and replacing them with product molecules. The position of the product molecules is carefully adjusted to make sure that the total energy change of the system corresponds to the reaction exothermicity. The CGCR model has been applied to simulations of laser irradiation of chlorobenzene at fluences such that there is ablation or massive removal of material. Two simulations, one for photothermal ablation and one for photochemical ablation, are compared to each other and to experimental data. In the photothermal simulation, all the laser energy goes into heat. In the photochemical simulation, the photon cleaves the C−Cl bond creating two radicals that can undergo subsequent abstraction and radical−radical recombination reactions.

Introduction

Computer modeling is playing an increasingly important role in the development of a better understanding of complex multiscale phenomena, for example, laser ablation of organic solids. The processes that occur in laser ablation can include primary elementary excitations of optically active states in the material, intramolecular vibrational equilibration, photochemical fragmentation of the excited molecule, intermolecular energy transfer, formation of highly energetic high-temperature and high-pressure regions, spallation of material, explosive disintegration and prompt forward ejection of a volume of material, intensive processes in the ejected plume, bond making/breaking chemical reactions in the target and in the plume, propagation of a pressure wave to the bottom of the target, and ionization. To complicate the situation even further, the processes occur at different time and length scales. The challenge to address all the relevant physics and chemistry within a single computational methodology is daunting. First, because of the collective character of laser ablation, exponential absorption of light into material, and pressure wave propagation into the material, a large molecular system of several hundred thousand molecules or more is needed. Second, a long real time needs to be simulated to account for the laser pulse, mechanical and thermal relaxation of material, and plume evolution. Third, to address chemical changes, available interaction potentials for all the photoinduced reaction intermediates and products are required. Finally, multiple long simulations of large systems with various laser fluences need to be performed. To provide an adequate description of laser ablation phenomena, a strategy is needed to model a large system for a long time and to include chemical reactions. Motion of particles is an essential feature of ablation; thus, the strategy for modeling must be based on a molecular dynamics (MD) approach that gives time dependent quantities. Below we describe various approaches at expanding the time and length scale of atomistic simulations and our logic for development of our new coarse-grained chemical reaction model (CGCRM).

Coarse-grained approaches can overcome time and length limitations of atomistic simulations while retaining significant microscopic information. The main idea of coarse-grained models is to ignore nonessential parts of the system or replace parts of the system with a larger scale computational model. One very successful strategy is to reduce the number of particles as in the united atom approximation and the bead-and-spring model in polymers in which a group of atoms is replaced by one unit. The unit can represent a chemical group of a few atoms, an entire molecule or a monomer unit in a polymer, groups of monomers, or chain segments of various lengths. For example, in our own mesoscale model of laser ablation each organic molecule such as dihydroxybenzoic acid is replaced by a spherical particle, which increases the simulation size by at least 20-fold in volume and 50-fold in time over atomistic simulations.[1−4] In modeling vesicle fusion, the small groups of atoms in lipids were represented as single interaction centers and four water molecules were represented by one particle, thus enabling the study of near atomic details during fusion.[5] Although the united atom simulations have been extremely successful, the incorporation of chemical reactions is not possible because simulation particles are not the real species and an interaction potential is not defined.

Another strategy to increase the length scale of the simulation is to combine computational methods. To examine long-range strain around a defect or crack in a solid, for example, atomistic simulations have been connected to a finite element method

* Corresponding author.

10.1021/jp035730i CCC: $27.50
Published on Web 01/17/2004

(FEM) in the boundary region.[6,7] A combination of molecular dynamics (MD), molecular statistics, kinetic lattice Monte Carlo, and continuum mechanics approaches tackles radiation damage in reactor steels.[8] The MD-FEM approach allows for chemical reactions such as fracture throughout the entire atomistic zone if an appropriate classical interaction potential is used. The developed interaction potentials that allow for reactions, however, are mainly for atomic systems.[9] One two-component reactive potential is the Brenner REBO potential for hydrocarbons.[10] In general, however, the number of chemically reactive interaction potentials is very limited.

For systems in which the chemical reaction zone is confined to tens of atoms, combined potentials, which use a quantum mechanical (QM) calculation for describing the forces in the reactive region and a classical molecular mechanics (MM) potential in the extended area, have been developed.[11] Numerous groups have been working on QM/MM approaches,[12] especially for systems of biological interest. For crack propagation in solids the QM/MM approach has been combined with an FEM boundary region.[13] The QM/MM calculations are typically performed for processes in which the atoms involved in the reaction are known in advance and the reaction center is reasonably well localized. The QM/MM approach is not feasible, however, if reactions are occurring throughout the large scale simulation system. Moreover, if a course-grained description of particles such as the united atom or the breathing sphere method is used, exact quantum mechanical descriptions of reactions cannot be defined. The challenge remains to develop a protocol for inclusion of widespread chemical reactions in a coarse-grained method.

Monte Carlo (MC) methods allow random chosen events, including reactions, to occur probabilistically. The input quantities can be relative energies and rates rather than an interaction potential. The kinetic MC (KMC) method has been used to study the importance of surface chemical reactions in simulations of the chemical vapor deposition of thin films,[14,15] defect reaction kinetics,[16] and thin film morphology.[17] The direct simulations MC method has been employed to simulate ultrafast detonations in chemical reaction systems.[18] A combination of the KMC method and continuum models has been used to increase the time of calculations in studies of epitaxial growth.[19] A hybrid MD-KMC method has been used to model hyperthermal deposition, in which the atomistic MD is used to simulate the complexity of the atomic collisions and KMC is used for the surface diffusion.[20] MC methods, however, do not provide direct access to dynamic behavior of the system, and do not yield dynamic quantities such as transport coefficients and time correlation functions.

For the simulation of laser ablation the coarse-grained (united atom) MD method is combined with the KMC philosophy. The beauty of MD simulations is once a force-field or interaction potential is specified, all dynamical motions of the particles follow logically by integrating the classical equations of motion. The results of the simulations, such as radial, velocity autocorrelation, energy, and angular distributions, can be directly compared with experimental quantities. Furthermore, the time dependence of the particle positions provides a microscopic view of motions that explains the macroscopic results. Analogous to KMC, the reaction events are described only by reaction probabilities and their overall energies, thus enabling the incorporation of chemical reactions into a coarse-grained MD model.

The coarse-grained chemical reaction model (CGCRM) for including the effects of chemical reactions is first implemented in the breathing sphere MD simulations of laser ablation.[21−24] The CGCR model uses as input known chemistry for the system under investigation and determines the effect of these chemical reactions on the process of interest. Our interest is the effect of photoinduced chemical reactions on the laser ablation phenomenon. We are not interested in predicting which chemical reactions occur but rather in describing how the reactions affect such properties as the amount of material removed as a function of laser fluence, the composition, angular and velocity distributions of the particles in the plume, and the strength of the acoustic pressure wave that is formed. Of particular note is that the photoinduced chemical reactions are exothermic; thus, considerable heat can be added to the system without direct relation to the laser fluence. In addition to heat changes, the composition of the system can alter the equilibrium density creating additional perturbations to the system.

Below we describe the CGCR model and its application to photochemical ablation of chlorobenzene. The main physical concept extracted from the simulations is that the temporal and spatial distributions of deposited enthalpy/heat are significantly different from the Beer's law deposition of laser energy during the laser pulse. The ramifications of these changes in enthalpy/heat deposition on experimentally measured quantities are briefly explained.

Coarse-Grained Chemical Reaction Model

Before explaining the CGCR model within the context of photochemical ablation of organic solids, a brief description of our mesoscale breathing sphere MD model of photothermal ablation is required.[1,2] Laser ablation is a collective and dynamic process and, thus, requires simulation of hundreds of thousands of molecules for at least a nanosecond. The essential approximation of our breathing sphere model is that each molecule is represented by a spherical particle that has true translational degrees of freedom but an approximate internal degree of freedom, that is, the breathing mode. For photothermal ablation, the photon from the laser is deposited into kinetic energy of the breathing mode. The potential parameters of the breathing mode are established in order to have a reasonable rate of energy transfer from the excited molecule to the remaining solid. The laser irradiation is simulated by randomly choosing molecules during the laser pulse of finite time duration with exponential attenuation of the laser light with depth modulated by Beer's law. The possible configurations that arise in the laser ablation simulation are shown in the time snapshots in Figure 1a,c,e,g. The laser impinges the sample from the right. The material on the right undergoes melting, explosive boiling, and removal by ablation, whereas the material at the left of the system remains a solid. The results of the simulations of photothermal ablation have been successfully compared to a vast array of experimental quantities.[2−4] The main conceptual prediction from the ablation simulations is that there is a clear threshold between desorption and ablation and that ablation necessarily has clusters of particles in the plume.[25] The predictions of the simulations regarding the pressure waves into the solid have recently been confirmed by experimental results.[26]

Another outcome of the photon absorption event is a direct scission of a chemical bond in the excited molecule. The excited molecule in this case breaks into free radicals, which are highly reactive and can subsequently undergo abstraction and recombination reactions. In our breathing sphere model we consider a whole molecule as a particle; therefore, we desired a method to split the particle into radicals and to include the occurrence of various chemical reactions. Consistent with the spirit of the breathing sphere model, we want to include the essential

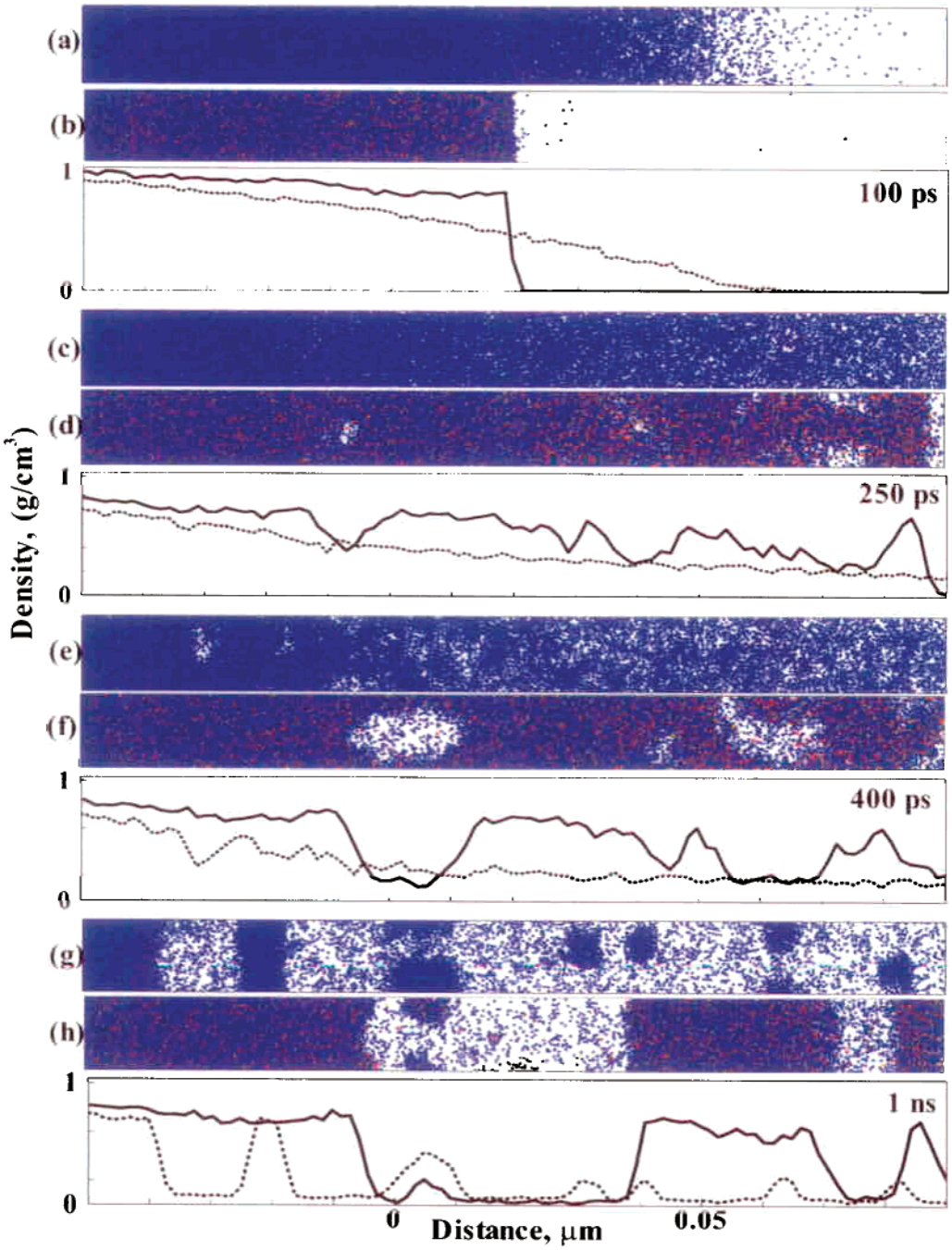

Figure 1. Plume development for the photothermal and photochemical simulations at several times in the near-surface region. The density is given by a solid line for the photochemical simulation and a dashed line for the photothermal simulation. The laser impinges from the right. The original surface is at 0. The penetration depth is 50 nm (0.05 μm) and is at the left most edge of the diagram. The blue dots represent the unreacted species; the other color dots are various reaction products. (a) Photothermal ablation at 100 ps. (b) Photochemical ablation at 100 ps. (c) Photothermal ablation at 250 ps. (d) Photochemical ablation at 250 ps. (e) Photothermal ablation at 400 ps. (f) Photochemical ablation at 400 ps. (g) Photothermal ablation at 1 ns. (h) Photochemical ablation at 1 ns.

information and data on the chemical reactions and omit time-consuming details. As in the KMC method, the essential pieces of information that we need are enthalpies and dynamics/probabilities of reactions. Therefore, we chose a specific compound to model. The chemical reaction patterns in our model presented in this paper are based on the known photochemistry of chlorobenzene.[21−24] The selection of chlorobenzene as the basic system for modeling photochemical events is based on the well-known photochemistry of the compound and extensive experimental ablation studies[27−32] that make a detailed interpretation and verification of the simulation results possible. Photofragmentation of chlorobenzene occurs via scission of the C−Cl bond to yield C_6H_5 and Cl radicals, which in solution and static gas cell experiments react with each other and with the parent molecule to form a number of different products.[27−29,33]

To represent the photochemical processes in chlorobenzene, we chose reactions that are thermodynamically favorable and are observed in gas-phase or solution chemistry of chlorobenzene. In total there are 12 reactions considered,[21] a sample of which is delineated below. For the exothermicity of the photofragmentation step, a photon wavelength of 248 nm (482.7 kJ/mol) is assumed. For convenience of interpretation, all energies are given in kJ/mol.

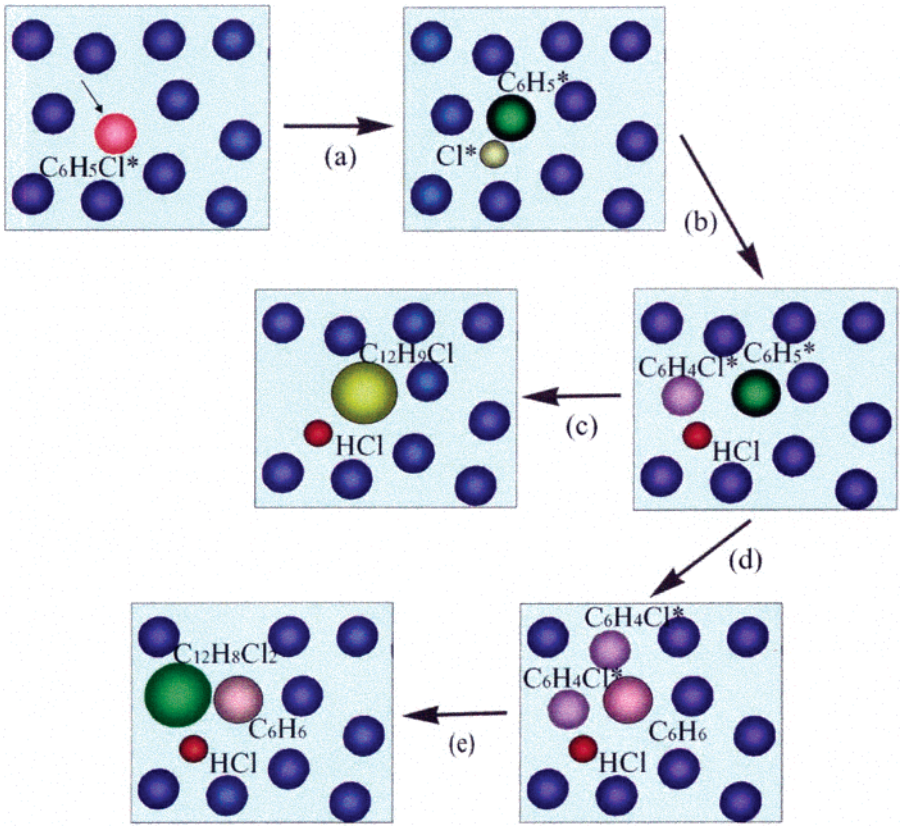

Figure 2. Schematic representation of the treatment of the various reaction types in the CGMCR simulation. Individual steps are described in the text.

• Laser excitation of the molecule:

$$C_6H_5Cl + h\nu \rightarrow C_6H_5Cl^*$$

• Photochemical decomposition of the excited molecule, that is, homolytic bond cleavage, step a in Figure 2:

$$C_6H_5Cl^* \rightarrow C_6H_5^{\bullet} + {}^{\bullet}Cl \qquad \Delta H_{rxn}{}^0 = -79.5 \text{ kJ/mol}$$

• Abstraction reactions by primary radicals, steps b and d in Figure 2:

$$C_6H_5Cl + {}^{\bullet}Cl \rightarrow C_6H_4Cl^{\bullet} + HCl$$
$$\Delta H_{rxn}{}^0 = \text{from } -109.3 \text{ to } -66.4 \text{ kJ/mol}$$

$$C_6H_5Cl + C_6H_5^{\bullet} \rightarrow C_6H_4Cl^{\bullet} + C_6H_6$$
$$\Delta H_{rxn}{}^0 = \text{from } -144.9 \text{ to } -136.5 \text{ kJ/mol}$$

• Radical−radical recombination reactions, steps c and e in Figure 2:

$$C_6H_4Cl^{\bullet} + {}^{\bullet}C_6H_5 \rightarrow C_{12}H_9Cl \qquad \Delta H_{rxn}{}^0 = -410.9 \text{ kJ/mol}$$

$$C_6H_4Cl^{\bullet} + {}^{\bullet}C_6H_4Cl \rightarrow C_{12}H_8Cl_2$$
$$\Delta H_{rxn}{}^0 = -282.3 \text{ to } -194.0 \text{ kJ/mol}$$

For each reaction the standard heat of formation, $\Delta H_{rxn}{}^0$, is calculated from the available thermochemical data[34,35] and depends on whether the reaction is taking place in the solid, liquid, or gas phase. All of the reactions considered are exothermic; thus, the addition of photochemistry into the system converts energy that has been stored in chemical bonds into enthalpy (heat) available for influencing the ablation processes.

In our simulations, the occurrence of chemical reaction is represented by a change in the types of particles including mass, size, and chemical reactivity as well as a change of the total energy of the sample by $\Delta H_{rxn}{}^0$ of the specific reaction. The change of the total energy in the sample is performed by changing interaction potentials to those of the product species and adjusting their initial positions, kinetic energy, and internal energy. For each of the new intermediate and product species, the parameters of the corresponding interaction potential are determined on small test samples of the system. The challenge is to find a set of parameters such that when molecules are deleted and replaced in the scenarios shown in Figure 2, the energy of the sample changes by roughly $E_{photon} - E_{bond}$, for the initial photon event and by $\Delta H_{rxn}{}^0$ for other reactions. Complete lists of the reactions, energetics, and model parameters have been given previously.[21]

To control the reaction dynamics/probabilities in our simulations, we introduce the parameter, τ_l, which we refer to as the "reaction time". The reaction time parameter is assigned to each radical and reflects the combination of the reaction's activation energy, lifetime, and the relative reactivity of the radicals participating in reaction. The reaction time, τ_l, is used along with the proximity of neighboring reaction partners to determine whether a reaction occurs or not. For radical−radical recombination reactions (steps c and e in Figure 2), the activation energy is zero; thus, these reactions occur as soon as two radicals are within 3 Å of each other, that is, $\tau_l = 0$. If a radical does not encounter another radical during a certain time, τ_l, then the radical can abstract a hydrogen or chlorine atom from the nearest chlorobenzene or dichlorobenzene molecule within 3 Å (steps

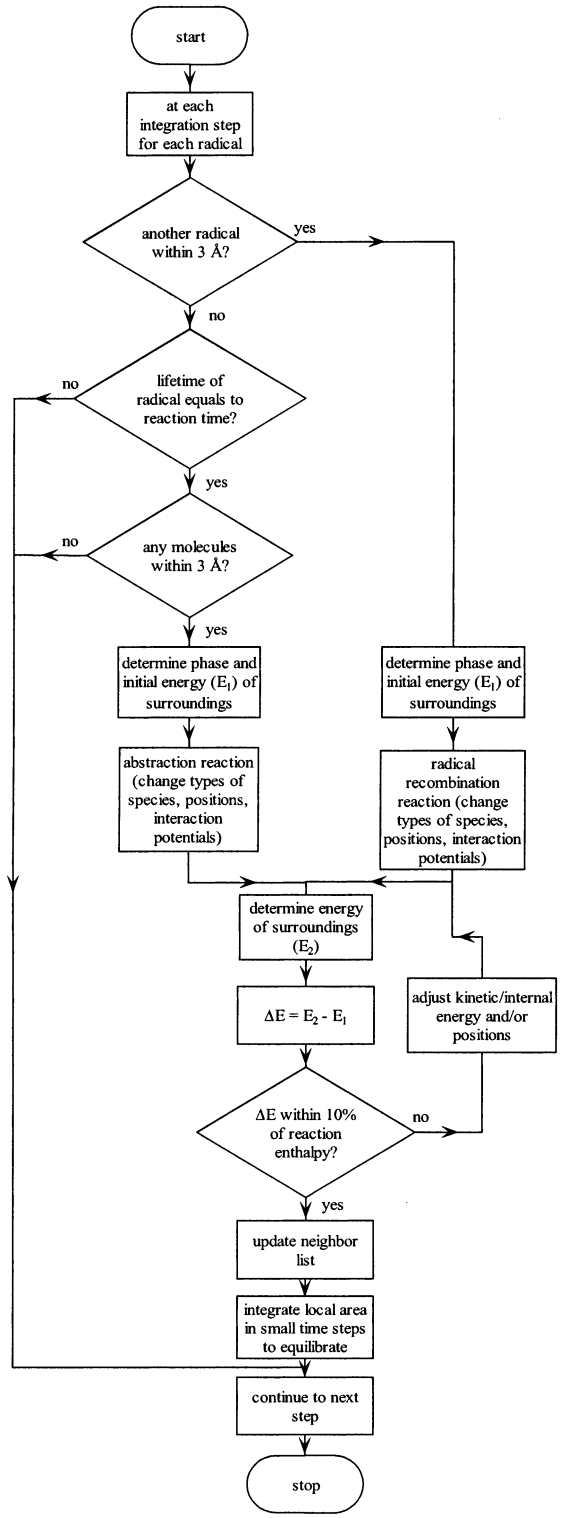

Figure 3. Flowchart for the coarse-grained chemical reaction model.

b and d in Figure 2). The reaction times for the abstraction reactions range from 0.3 (Cl radical) to 0.8 ps (C_6H_4Cl radical) in our simulations. More details of relative lifetimes were given previously.[21]

To describe the general CGCRM simulation, it is easiest to start after the end of the laser pulse. The initial condition is approximately that given in the top snapshots of Figure 1. The right side of the sample is melted and will shortly enter the gas phase; thus, the species are quite mobile. The steps in the CGCRM simulation are shown in the flowchart in Figure 3 and proceed as follows:

1. Track each reactive species, in this case, each radical.

2. At each time step, 5 fs in our simulations, check the vicinity of each radical for possible reaction partners and check the reaction time, τ_l.

- If two radicals are within 3 Å of each other, replace the two radicals by the product molecule.
- If a radical has lived sufficiently long to abstract an atom from a neighboring molecule within 3 Å, then a new molecule and new radical are created.

3. For each reaction site, determine the phase (solid, liquid, gaseous) of the surrounding area. Change the type of species and the interaction potentials. Adjust the position of the product molecule(s) so that the total energy change of the system is approximately ΔH_{rxn}^0. The energy change is carefully monitored by adjusting initial positions of the reaction products and by performing additional local energy checks. Kinetic and internal energy is added to the particles to ensure that the total energy change is within 10% of the exothermicity values.

4. Update the neighbor list to remove reactants and add products.

5. Integrate the particles in the regions where reactions are taking place at a reduced time step while holding the positions of the remaining particles fixed. This procedure equilibrates the reaction region to the remaining system. Typically the local region is equilibrated for 10 time steps at one-tenth the normal time step of the whole simulation.

For the duration of the laser pulse, the same protocol is implemented except that every few steps, depending on the fluence, a photon energy is absorbed and converted into vibrational excitation of a molecule or severs the phenyl−chloride bond as in step a in Figure 2.

The system is $10 \times 10 \times 191$ nm^3 with 126 950 chlorobenzene molecules. The laser wavelength is 248 nm (482.7 kJ/mol) with a penetration depth of 50 nm and a pulse width of 150 ps. Dynamic nonabsorbing boundary conditions are applied at the bottom of the sample to avoid artifacts due to the reflection of the laser-induced pressure wave from the edge of the computational cell.[36] Periodic boundary conditions in the direction parallel to the surface are imposed, simulating the conditions at the center of a laser spot. In this paper we discuss the results from two simulations. The first simulation assumes that molecules can only undergo photothermal excitation. The fluence is 86.69 J/m^2, a value that is well above the ablation threshold.[2] The second simulation is pure photochemical, that is, all photons react with the molecule to induce bond cleavage. The nominal laser fluence is 11 J/m^2. These conditions were chosen so that the total deposited enthalpy (heat) available for ablation processes is similar in the two simulations.

Results

Figure 1 shows snapshots of the plume in the near-surface region for the photothermal (frames a, c, e, and g) and photochemical (frames b, d, f, and h) ablation simulations as a function of time. The laser impinges the sample from the right. Below the snapshots of the plume is a density profile for the two simulations. The first time snapshot is at 100 ps and is before the end of the laser pulse. The system with photothermal deposition of energy exhibits considerable swelling, whereas the photochemical system has a sharp surface with a few desorbed molecules. The system with the photothermal deposition of energy continues to expand and undergoes explosive boiling[1,2] which results in a plume of individual molecules as well as liquid droplets as shown in the 1 ns snapshot, Figure 1g. For the most part the clusters are smaller than the width of

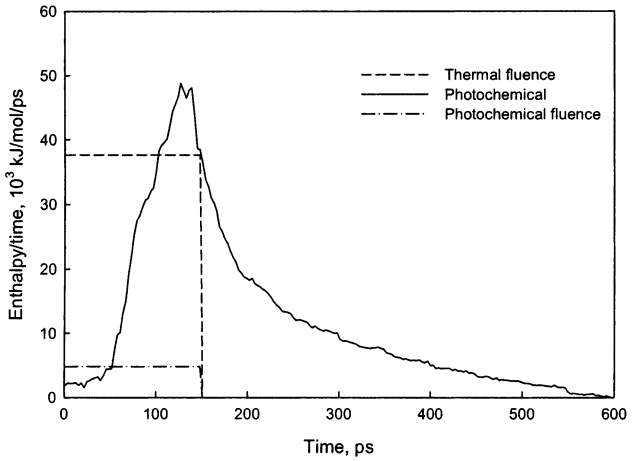

Figure 4. Enthalpy deposited per unit time vs time.

the simulation cell. In the photochemical process, on the other hand, the plume density is not as monotonic with height as shown for the 250 and 400 ps snapshots. The final clusters are larger than the width of the simulation cell. The appearance of voids at 400 ps, Figure 1f, is reminiscent of the photothermal simulations performed for very short laser pulses in which there is stress confinement and the emission of particles is from void formation and spallation.[1,2] Independent of fluence, the material removal, 43 nm for photochemical ablation and 50 nm for photothermal ablation, in both cases is approximately the same.

The calculations clearly delineate for the first time the fundamental differences between photothermal and photochemical ablation. The reasons for the differences in the plume as well as most of the comparisons with experimental data can be understood by examining the temporal and spatial distribution of enthalpy (heat) deposited in the system. Shown in Figure 4 is the temporal evolution of the enthalpy change per unit time. For the photothermal process the enthalpy change is uniform with time and reflects the laser fluence. The fluence for the photochemical simulation is also shown. This fluence would be below the ablation threshold for photothermal processes.[2] Also shown is the enthalpy change with photochemical processes included. Fluences are chosen such that the total enthalpy added in photothermal and photochemical simulations is the same. For the first third of the laser pulse, most of the photon energy is going into bond cleavage. Even by 100 ps, the time of the first snapshot in Figure 1b, the enthalpy deposited is considerably less than with the photothermal model; thus, it is not surprising that little expansion of the solid occurs. In the time period from 20 to 150 ps many chemical reactions are occurring leading to a rapid deposition of enthalpy. The conditions are similar to stress confinement in which the energy is deposited faster than the system can mechanically relax.[1,2] Thus, it is not surprising that the plume shown in snapshots f and h of Figure 1 have features similar to stress confinement. The other obvious feature shown in Figure 4 is that reactions continue after the end of the laser pulse, thus continuing to add heat during plume development. Overall the conversion of energy stored in chemical bonds to heat contributes about 7 times as much enthalpy as does the laser fluence.

Figure 5 shows the spatial distribution of enthalpy change. Figure 5a is for the photothermal process and has the Beer's law profile superimposed. This figure clearly shows that surface swelling occurs during the laser pulse and that considerable energy is deposited at 4 times the penetration depth, that is, at −200 nm. The enthalpy deposited for photon-induced bond cleavage and for exothermic abstraction and radical−radical

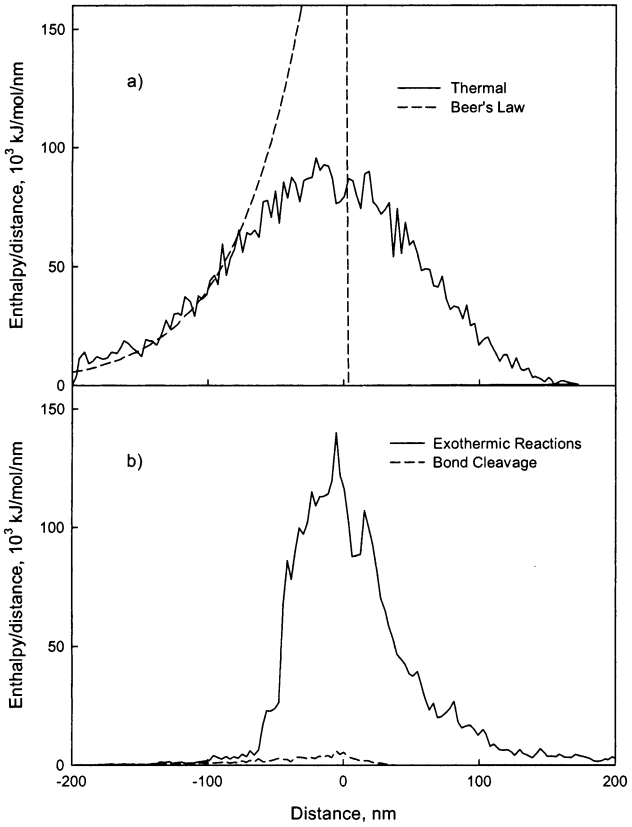

Figure 5. Enthalpy deposited per distance vs distance. (a) Photothermal process with Beer's law profile. (b) Photochemical process showing bond scission events separate from the exothermic abstraction and radical−radical recombination reactions.

recombination reactions are shown separately in Figure 5b for the photochemical simulation. In contrast to the photothermal simulation, the enthalpy deposited in the photochemical simulation is deposited almost exclusively within 60−70 nm of the surface. The radicals created deeper in the sample cannot diffuse and initiate the chain of exothermic reactions. The enthalpy deposited above the surface in this case corresponds to reactions in the plume at times beyond the end of the laser pulse.

The difference in the temporal and spatial deposition of energy available for the ablation physics in photochemical versus photothermal ablation is the new concept to arise from these calculations. This concept provides the foundation to make specific comparisons with experiment and to explain experimental results as summarized below and as explained previously in more detail.[21−24]

- The additional energy release in exothermic reactions initiated by photochemistry results in a lower ablation threshold with photochemical ablation than pure photothermal ablation.[37−40]
- The fast rise of energy deposition in time from 20 to 150 ps explains the presence of a shock wave with a high initial velocity,[30,31,41,42] large clusters in the plume, and high velocities of particles in the plume.[43,44]
- The ongoing chemical reactions above the surface after the laser pulse explain the higher background density in the plume with photochemical ablation than with photothermal ablation.[42]
- The association of a thermal mechanism of material removal below the ablation threshold and a volume ejection mechanism above threshold[1,2] explains why nonvolatile products such as HCl and the matrix are only observed below threshold and all products are observed above threshold.[27,45]
- The lack of heat deposited below ∼1.5 times the penetration depth as shown in Figure 5b may help explain the cold-etching

process in far-UV photoablation[46,47] as is used commercially in the corrective eye surgery, LASIK.[48]

Conclusion

We have developed a coarse-grained chemical reaction model, CGCRM, to incorporate the effects of chemistry on a physical process, in this case, laser ablation. The system size investigated contained 130 000 molecules, that is, effectively about 1.5×10^6 atoms, in a 1.9×10^4 nm^3 volume. The molecules could undergo 12 different reactions throughout the entire simulation volume resulting in a total of 111 790 chemical reactions for the laser fluence discussed in this paper.[21] Simulations for many laser fluences have been calculated[21−24] with each simulation taking approximately 1 month on a 4-way SMP IBM SP processor.[49] The predictions from the simulations compare favorably with a diverse array of experimental data.

The proposed methodology can be applied to many large scale applications. Currently we are incorporating it into another coarse-grained model, that is, the united atom model, to examine photochemical changes in a poly(methyl methacrylate) (PMMA) polymer due to UV irradiation for applications such as laser surgery and the irradiation damage of objects in low earth orbit. We are planning to employ this methodology in a study of ionization of water molecules due to energetic particle bombardment.[50] Other potential applications of the methodology include examining the effects of changes in heat and composition due to chemical reactions in detonation of explosives and in propulsion in rocket engines. For other applications, complex temperature dependencies of the chemical reaction probabilities can be used.

Acknowledgment. This work was supported by the U.S. Air Force Office of Scientific Research through the Medical Free Electron Laser program and the Multi-University Research Initiative as well as the Chemistry Division of the National Science Foundation. We thank Professor Leonid Zhigilei of the University of Virginia for many helpful discussions.

References and Notes

(1) Zhigilei, L. V.; Kodali, P. B. S.; Garrison, B. J. *J. Phys. Chem. B* **1997**, *101*, 2028; **1998**, *102*, 2845.
(2) Zhigilei, L. V.; Garrison, B. J. *J. Appl. Phys.* **2000**, *88*, 1281.
(3) Zhigilei, L. V.; Leveugle, E.; Garrison, G. J.; Yingling, Y. G.; Zeifman, M. I. *Chem. Rev.* **2003**, *103*, 321.
(4) Zhigilei, L. V.; Yingling, Y. G.; Itina, T. E.; Schoolcraft, T. A.; Garrison, B. J. *Int. J. Mass Spectrom. Ion Processes* **2003**, *226*, 85.
(5) Marrink, S. J.; Mark, A. E. *J. Am. Chem. Soc.* **2003**, *125*, 11145.
(6) Tadmor, E. B.; Ortiz, M.; Phillips, R. *Philos. Mag. A.* **1996**, *73*, 1529.
(7) Rudd, R. E.; Broughton, J. Q. *Phys. Rev. B* **1998**, *58*, R5893.
(8) Odette, G. R.; Wirth, B. D.; Bacon, D. J.; Ghoniem, N. M. *MRS Bull.* **2001**, *26*, 176.
(9) Garrison, B. J.; Srivastava, D. *Annu. Rev. Phys. Chem.* **1995**, *46*, 373.
(10) (a) Brenner, D. W. *Phys. Rev. B* **1990**, *42*, 9458. (b) Brenner, D. W.; Shenderova, O. A.; Harrison, J. A.; Stuart, S. J.; Ni, B.; Sinnott, S. B. *J. Phys.: Condens. Matter* **2002**, *14*, 783.
(11) Baschnagel, J.; Binder, K.; Doruker, P.; Gusev, A. A.; Hahn, O.; Kremer, K.; Mattice, W. L.; Muller-Plathe, F.; Murat, M.; Paul, W.; Santos, S.; Suter, U. W.; Tries, V. *Adv. Polym. Sci.* **2000**, *152*, 41.
(12) See for example: (a) Singh, U. C.; Kollman, P. A. *J. Comput. Chem.* **1986**, *7*, 718. (b) Field, M. J.; Bash, P. A.; Karplus, M. *J. Comput. Chem.* **1990**, *11*, 700. (c) Gao, J. *Rev. Comput. Chem.* **1995**, *7*, 119. (d) Bakowies, D.; Thiel, W. *J. Comput. Chem.* **1996**, *17*, 87. (e) Monard, G.; Merz, K. M., Jr. *Acc. Chem. Res.* **1999**, *32*, 904.
(13) Broughton, J. Q.; Abraham, F. F.; Bernstein, N.; Kaxiras, E. *Phys. Rev. B* **1999**, *60*, 2391.
(14) Dawnkaski, E. J.; Srivastava, D.; Garrison, B. J. *J. Chem. Phys.* **1996**, *104*, 5997.
(15) Battaile, C. C.; Srolovitz, D. J.; Butler, J. E. *J. Appl. Phys.* **1997**, *82*, 6293.
(16) Heinisch, H. L.; Singh, B. N. *Fusion Mater.* **2002**, *33*, 146.
(17) Merrick, M. L.; Luo, W.; Fichthorn, K. A. *Prog. Surf. Sci.* **2003**, *72*, 117.
(18) Anderson, J. B.; Long, L. N. *J. Chem. Phys.* **2003**, *118*, 3102.
(19) Schulze, T. P.; Smereka, P.; Weinan, E. *J. Comput. Phys.* **2003**, *189*, 197.
(20) Pomeroy, J. M.; Jacobsen, J.; Hill, C. C.; Cooper, B. H.; Sethna, J. P. *Phys. Rev. B* **2002**, *66*, 235412.
(21) Yingling, Y. G.; Zhigilei, L. V.; Garrison, B. J. *J. Photochem. Photobiol., A* **2001**, *145*, 173−181.
(22) Yingling, Y. G.; Zhigilei, L. V.; Garrison, B. J. *Nucl. Instrum. Methods Phys. Res., Sect. B* **2001**, *180*, 171−175.
(23) Yingling, Y. G.; Garrison, B. J. *Nucl. Instrum. Methods Phys. Res. B* **2003**, *203*, 188.
(24) Yingling, Y. G.; Garrison, B. J. *Chem. Phys. Lett.* **2002**, *364*, 237.
(25) Georgiou, S.; Hillenkamp, F. *Chem. Rev.* **2003**, *103*, 317.
(26) Rohlfing, A.; Menzel, C.; Kukreja, L. M.; Hillenkamp, F.; Dreisewerd, K. *J. Phys. Chem. B* **2003**, *107*, 12275.
(27) Georgiou, S.; Koubenakis, A.; Syrrou, M.; Kontoleta, P. *Chem. Phys. Lett.* **1997**, *270*, 491.
(28) Georgiou, S.; Koubenakis, A.; Labrakis, J.; Lassithiotaki, M. *J. Chem. Phys.* **1998**, *109*, 8591.
(29) Georgiou, S.; Koubenakis, A.; Labrakis, J.; Lassithiotaki, M. *Appl. Surf. Sci.* **1998**, *127*, 122.
(30) Tsuboi, Y.; Hatanaka, K.; Fukumura, H.; Masuhara, H. *J. Phys. Chem.* **1994**, *98*, 11237.
(31) Tsuboi, Y.; Hatanaka, K.; Fukumura, H.; Masuhara, H. *J. Phys. Chem. A* **1998**, *102*, 1661.
(32) Ichimura, T.; Mori, Y.; Shinohara, H.; Nishi, N. *Chem. Phys.* **1994**, *189*, 117.
(33) Davidson, R. S.; Goodin, J. W.; Kemp, G. *Adv. Phys. Org. Chem.* **1984**, *20*, 191 and references therein.
(34) National Institute of Standards and Technology online databases. http://www.nist.gov/srd/online.html.
(35) Yim, Y. H.; Kim, M. S. *J. Phys. Chem.* **1994**, *98*, 5201.
(36) Zhigilei, L. V.; Garrison, B. J. *Mater. Res. Symp. Soc. Proc.* **1999**, *538*, 491.
(37) Lippert, T.; David, C.; Dickinson, J. T.; Hauer, M.; Kogelschatz, U.; Langford, S. C.; Nuyken, O.; Phipps, C.; Robert, J.; Wokaun, A. *J. Photochem. Photobiol., A* **2001**, *145*.
(38) Lippert, T.; David, C.; Hauer, M.; Masubuchi, T.; Musuhara, H.; Nomura, K.; Nuyken, O.; Phipps, C.; Robert, J.; Tada, T.; Tomita, K.; Wokaun, A. *Appl. Surf. Sci.* **2001**, *186*, 145.
(39) Wei, J.; Hoogen, N.; Lippert, T.; Nyuken, O.; Wokaun, A. *J. Phys. Chem. B* **2001**, *105*, 1267.
(40) Masubuchi, T.; Fukumura, H.; Masuhara, H.; Suzuki, K.; Hayashi, N. *J. Photochem. Photobiol,. A* **2001**, *145*, 215.
(41) Tsuboi, Y.; Fukumura, H.; Masuhara, H. *J. Phys. Chem.* **1995**, *99*, 10305.
(42) Hatanaka, K.; Kawao, M.; Tsuboi, Y.; Fukumura, H. *J. Appl. Phys.* **1997**, *82*, 5799.
(43) Lippert, T.; Dickinson, J. T.; Langford, S. C.; Furutani, H.; Fukumura, H.; Masuhara, H.; Kunz, T.; Wokaun, A. *Appl. Surf. Sci.* **1998**, *127*, 117.
(44) Tanaka, K.; Miyajima, T.; Shirai, N.; Zhuang, Q.; Nakata, R. *J. Appl. Phys.* **1995**, *77*, 6581.
(45) Yingling, Y. G.; Zhigilei, L. V.; Garrison, B. J.; Koubenakis, A.; Labrakis, J.; Georgiou, S. *Appl. Phys. Lett.* **2001**, *78*, 1631.
(46) Srinivasan, R.; Braren, B. *Chem. Rev.* **1989**, *89*, 1303.
(47) Garrison, B. J.; Srinivasan, R. *J. Appl. Phys.* **1985**, *57*, 2909−2914. A picture of the effect of photothermal ablation vs photochemical ablation on etching of an aortal wall is included.
(48) Gorman, C. RU Ready to Dump Your Glasses? Laser Surgery Can Work Wonders but There Are Risks. *Time*, October 11, 1999.
(49) Graduate Education and Research Services, High Performance Computing Group. http://gears.aset.psu.edu/hpc/systems/ibmsp/.
(50) Wojciechowski, I. A.; Sun, S.; Szakal, C.; Winograd, N.; Garrison, B. J. *J. Phys. Chem.* A, in press.